Cancer Letters 598 (2024) 217091

Contents lists available at ScienceDirect

Cancer Letters

journal homepage: www.elsevier.com/locate/canlet

Original Articles

MCT1-dependent lactate recycling is a metabolic vulnerability in colorectal cancer cells upon acquired resistance to *anti*-EGFR targeted therapy

Elena Richiardone [a], Rim Al Roumi [a], Fanny Lardinois [b], Maria Virginia Giolito [a], Jérôme Ambroise [c], Romain Boidot [d], Bernhard Drotleff [e], Bart Ghesquière [f,g], Akeila Bellahcène [b], Alberto Bardelli [h,i], Sabrina Arena [j,k,**], Cyril Corbet [a,*]

[a] *Pole of Pharmacology and Therapeutics (FATH), Institut de Recherche Expérimentale et Clinique (IREC), UCLouvain, Avenue Hippocrate 57, B1.57.04, B-1200, Brussels, Belgium*
[b] *Metastasis Research Laboratory, GIGA Cancer, University of Liège, Liège, Belgium*
[c] *Centre des Technologies Moléculaires Appliquées (CTMA), Institut de Recherche Expérimentale et Clinique (IREC), UCLouvain, Avenue Hippocrate 54, B-1200, Brussels, Belgium*
[d] *Unit of Molecular Biology, Department of Biology and Pathology of Tumors, Georges-François Leclerc Cancer Center-UNICANCER, 21079, Dijon, France*
[e] *Metabolomics Core Facility, EMBL Heidelberg, Heidelberg, Germany*
[f] *Laboratory of Applied Mass Spectrometry, Department of Cellular and Molecular Medicine, KU Leuven, Leuven, Belgium*
[g] *Metabolomics Core Facility Leuven, Center for Cancer Biology, VIB, Leuven, Belgium*
[h] *Department of Oncology, Molecular Biotechnology Center, University of Torino, Torino, Italy*
[i] *IFOM ETS - the AIRC Institute of Molecular Oncology, Milan, Italy*
[j] *Department of Oncology, University of Torino, Candiolo, TO, Italy*
[k] *Candiolo Cancer Institute, FPO-IRCCS, Candiolo, TO, Italy*

ARTICLE INFO

Keywords:
Colorectal cancer
Metabolism
Therapy resistance
KRAS
Cetuximab
Lactate
Monocarboxylate transporter

ABSTRACT

Despite the implementation of personalized medicine, patients with metastatic CRC (mCRC) still have a dismal overall survival due to the frequent occurrence of acquired resistance mechanisms thereby leading to clinical relapse. Understanding molecular mechanisms that support acquired resistance to *anti*-EGFR targeted therapy in mCRC is therefore clinically relevant and key to improving patient outcomes. Here, we observe distinct metabolic changes between cetuximab-resistant CRC cell populations, with in particular an increased glycolytic activity in *KRAS*-mutant cetuximab-resistant CRC cells (LIM1215 and OXCO2) but not in *KRAS*-amplified resistant DiFi cells. We show that cetuximab-resistant LIM1215 and OXCO2 cells have the capacity to recycle glycolysis-derived lactate to sustain their growth capacity. This is associated with an upregulation of the lactate importer MCT1 at both transcript and protein levels. Pharmacological inhibition of MCT1, with AR-C155858, reduces the uptake and oxidation of lactate and impairs growth capacity in cetuximab-resistant LIM1215 cells both *in vitro* and *in vivo*. This study identifies MCT1-dependent lactate utilization as a clinically actionable, metabolic vulnerability to overcome *KRAS*-mutant-mediated acquired resistance to *anti*-EGFR therapy in CRC.

1. Introduction

Colorectal cancer (CRC) represents a prototypical cancer for which therapy resistance contributes to poor prognosis due to rapid clinical relapse. First-line options for treating patients with metastatic CRC (mCRC) include the use of cetuximab or panitumumab, two anti-epidermal growth factor receptor (EGFR) monoclonal antibodies (mAbs). Although they significantly improve progression-free survival and median overall survival when combined with chemotherapy [1–3], *anti*-EGFR mAbs achieve very limited (<10 %) objective response rates in unselected CRC patients when given in monotherapy [4]. Despite EGFR (over)expression in about 85 % of patients with mCRC, the clinical applicability of such mAbs is restricted to a subset of them (<40 %) [5]. Indeed, genetic alterations, associated with primary and acquired resistance to *anti*-EGFR therapies, are very diverse, thereby limiting the success of such targeted agents. Activating mutations within *KRAS*,

* Corresponding author.
** Corresponding author.
E-mail addresses: sabrina.arena@unito.it (S. Arena), cyril.corbet@uclouvain.be (C. Corbet).

https://doi.org/10.1016/j.canlet.2024.217091
Received 17 April 2024; Received in revised form 11 June 2024; Accepted 25 June 2024
Available online 2 July 2024

NRAS and *BRAF* genes have been significantly associated with a lack of response to *anti*-EGFR therapy in patients with mCRC. Moreover, other gene alterations (e.g. *MET* amplification, *PIK3CA* activating mutations, *PTEN* loss-of-function mutations) have been reported to affect response to EGFR-targeting mAbs [6,7]. Altogether, these observations underscore the complexity (and limitation) of genomic profiling for clinical decision-making for mCRC patients and the urgent need to implement fundamental changes in the tumor treatment paradigm by the development of new therapeutic options that can help to prevent or overcome the occurrence of clinical drug resistance.

Dysregulated cell metabolism is a common hallmark of cancer and it has emerged as an important factor that contributes to disease progression and clinical relapse in cancer patients, including CRC [8–10]. Metabolic preferences in cancer cells can continuously evolve to fulfil their bioenergetic and biosynthetic needs and to support their growth and survival when facing hostile conditions, including therapy-induced stress [11]. Several recent studies have shown that cancer cells acquiring resistance to targeted agents display a profound metabolic reprogramming [12–15]; however metabolic liabilities that may improve the response to *anti*-EGFR therapy have not been clearly identified yet in CRC. In this study, we postulated that long-term exposure to cetuximab could account for substantial changes of metabolic preferences in CRC cells, which may be therapeutically exploited to overcome secondary drug resistance. We found that metabolic rewiring was profoundly different between CRC cells that harbor distinct resistance-causing genetic alterations, with enhanced glycolysis as a common feature for *KRAS*-mutant cetuximab-resistant CRC cells. We further revealed that these cells had the capacity to recycle glycolysis-derived lactate, in a MCT1-dependent manner, to sustain their growth capacity in presence of *anti*-EGFR therapy. Finally, we documented that pharmacological inhibition of MCT1 significantly reduced the growth of cetuximab-resistant CRC, in both *in vitro* and *in vivo* conditions, by preventing the use of lactate as an alternative energy fuel.

2. Material and methods

2.1. Cell lines and culture

Human colorectal DiFi, LIM1215 and OXCO2 cancer cell lines (both parental and resistant derivatives) were obtained from Prof Alberto Bardelli, University of Torino, Italy. LIM1215 parental cell line had been described previously [16] and was obtained from Prof Robert Whitehead, Vanderbilt University, Nashville, with permission from the Ludwig Institute for Cancer Research, Zurich, Switzerland. The DiFi and OXCO2 cell lines were a kind gift from Dr. J. Baselga in November 2004 (Oncology Department of Vall d'Hebron University Hospital, Barcelona, Spain) and Dr V. Cerundolo in March 2010 (Weatherall Institute of Molecular Medicine, University of Oxford, Oxford, United Kingdom), respectively. Cetuximab-resistant DiFi and LIM1215 cancer cells were established as previously described [17]. Briefly, DiFi-R1 cell population was obtained after exposure of the parental DiFi cells, to a constant dose of cetuximab (350 nM), for one year. DiFi-R2 cells were established by increasing cetuximab dosage stepwise starting from 3.5 nM to 35 nM and finally to 350 nM during a time of one year. Similar protocols were applied to LIM1215 cells, for at least 3 months' drug treatment, with variations regarding cetuximab concentrations: 1400 nM cetuximab for LIM1215-R1 cell selection while drug concentration started from 350 nM, to 700 nM and finally 1400 nM for LIM1215-R2 cells. OXCO2-R6 cell population was generated upon continuous treatment with 50 μg/mL cetuximab. Cell lines were stored according to the supplier's instructions and used within 6 months after resuscitation of frozen aliquots. DiFi cells were cultured in Dulbecco's Modified Eagle Medium/Nutrient Mixture F-12 (DMEM/F-12; #11330032, Thermo Fisher Scientific) while LIM1215 cells were grown in RPMI-1640 medium + GlutaMAX (#61870–010, Thermo Fisher Scientific). OXCO2 cells were grown in Iscove's Modified Dulbecco's Medium (IMDM, GlutaMAX™ supplement, #31980022, Thermo Fisher Scientific). Media were supplemented with 10 % heat-inactivated fetal bovine serum (FBS; F7524, Sigma-Aldrich), and 1 % penicillin-streptomycin (#15140163, Thermo Fisher Scientific), and cells were maintained in exponential growth in 5 % CO_2/95 % air in a humidified incubator at 37 °C. Cetuximab-resistant DiFi, LIM1215 and OXCO2 cancer cells were cultured under continuous treatment with 25 μg/mL cetuximab (Erbitux 5 mg/mL; Merck #L01XC06). All cell lines were tested for Mycoplasma contamination with the PCR-based MycoplasmaCheck service from Eurofins Genomics.

2.2. Cell treatment

Cell treatment was performed in a full culture medium with cetuximab, 3-BrPA (#16490, Sigma-Aldrich) or AR-C155858 (#533436, Sigma-Aldrich) for 72 h at different concentrations, as indicated in the figure legends. In some experimental conditions, cells were incubated for 72 h in a medium containing 10 mM sodium lactate (#71718, Sigma-Aldrich - instead of glucose) and 2 mM glutamine (#25030–024, Thermo Fisher Scientific). Cell growth was assessed either by direct cell counting on a hemocytometer with Trypan Blue exclusion dye or by using the Presto Blue reagent (#A13262; Thermo Fisher Scientific) according to manufacturer's instructions.

2.3. Migration assays

Migration assays were performed in 12-well Transwell microchambers (Corning) with 8-μm pore-sized membranes. Cells (3×10^4 cells/well; 3 wells/condition) were seeded in the upper chamber of the Transwells, in a serum-free medium. In some conditions (as described in figure legends), 20 μM AR-C155858 was added in the upper chamber for the time of the migration assay (24 h). A medium containing 10 % FBS was added in the lower chamber, and cells were allowed to migrate for 24 h at 37 °C. The Transwell membranes were then fixed with 4 % paraformaldehyde for 1 h at room temperature (RT) and stained with 0.5 % crystal violet in 10 % ethanol for 1 h at RT. Cells that had not migrated through the chamber were removed with a cotton swab. Migrating cells were imaged by brightfield microscopy with the Axiovert 100 (Zeiss) before quantification with QuPath-0.3.2 software.

2.4. In vivo tumor xenografts

All animal experimental procedures were performed according to the Federation of European Laboratory Animal Sciences Associations (FELASA) and were reviewed and approved by the Institutional Animal Care and Ethics Committee of the University of Liege (Ethics committee approval 19–2156). Animals were housed in the GIGA-accredited animal facility (University of Liege) under standard conditions (12 h light/dark cycle, light on at 7 a.m., food and water provided *ad libitum*). LIM1215-S and -R1 cells (3×10^6 cells/mouse) were suspended in FBS-free culture medium with Matrigel (1:1 ratio). Cell suspensions were injected subcutaneously into the right posterior flanks of 7-week-old immunodeficient NOD-SCID male mice purchased from Elevage Janvier. Tumor volume was monitored three times per week using caliper and was calculated using the ellipsoidal formula $V = 4/3 \times \pi \times (L/2)^2 \times w/2$ (L = length; w = width). When tumors reached a diameter of approximately 5 mm, AR-C155858 (3 mg/kg, resuspended in DMSO) was injected daily intraperitoneally. After 4 weeks of AR-C155858 treatment, mice were euthanized, and tumors were collected. Tumor growth index was calculated as follows: Volume day x -Volume day 0/ Volume day 0.

2.5. Western blot analysis

Subconfluent cancer cells were washed twice with ice-cold PBS and lysed in a RIPA buffer supplemented with phosphatase and protease inhibitor cocktails (#4906837001 and P8340, Sigma-Aldrich). Cell

lysates were then cleared by centrifugation (6000×*g*, 10 min, 4 °C) and stored at −80 °C until analysis. After determination of protein concentration using a bicinchoninic acid-based assay (Thermo Fisher Scientific), samples were denaturated (5 min, 95 °C) with Laemmli sample buffer containing 100 mM dithiothreitol. Samples (20 μg per well) were then separated by SDS-PAGE (8–15 % acrylamide/bis-acrylamide gels) and transferred to PVDF membranes. Membranes were blocked with 5 % bovine serum albumin (BSA) in TBS-0.1 % Tween 20 (TTBS) and subsequently immunoblotted overnight at 4 °C with specific primary antibodies against EGFR (#4267, 1:1000), Akt (#9272, 1:1000), phospho-Akt (Ser-473) (#4060, 1:1000), p44/42 MAPK (#9102, 1:1000) and phospho-p44/42 MAPK (Thr-202/Tyr-204) (#9101, 1:1000), all from Cell Signaling Technology; MCT1 (#AB3538P, Sigma-Aldrich, 1:500) and Hsp90 (#610419, BD Biosciences, 1:10,000). After several washes with TTBS, membranes were then incubated (1 h, RT) with horseradish peroxidase (HRP)-conjugated secondary antibodies (Jackson Immunoresearch) and chemoluminescent signals were revealed by using ECL Western Blotting Detection Kit (GE Healthcare) on X-ray films in a dark chamber or with an Amersham Imager 600 (GE Healthcare).

2.6. RNA sequencing

Total RNA was extracted from frozen cell pellets with the Monarch Total RNA Miniprep kit (New England Biolabs) by following manufacturer's protocol. Total RNA (300 ng/sample) was ribodepleted by using the NEBNEXT rRNA Depletion kit (New England Biolabs) according to manufacturer's instructions. Ribodepleted RNA was then used for the library preparation with the NEBNext Ultra II Directional RNA library prep kit for Illumina (New England Biolabs) according to manufacturer's instructions. Libraries were paired-end sequenced (2 × 100 base pairs) on a NextSeq2000 device (Illumina), with a minimal depth of 10 million reads. All sequencing data were analyzed using the Automated Reproducible MOdular workflow for preprocessing and differential analysis of RNA-seq data (ARMOR v1.5.4) pipeline [18]. In this pipeline, reads underwent a quality check using FastQC (Babraham Bioinformatics). Quantification and quality control results were summarised in a MultiQC report before being mapped using Salmon [19] to the transcriptome index which was built using all Ensembl cDNA sequences obtained in the Homo_sapiens.GRCh38.cdna.all.fa file. Then, estimated transcript abundances from Salmon were imported into R using the tximeta package [20] and analyzed for differential gene expression with edgeR [21].

2.7. Dosage of extracellular glucose and lactate

Cancer cells (2 × 10^5 cells/well; 3 wells/condition) were seeded in 12-well plates with 1 mL of their routine culture medium. After 24 h, medium was replaced by 500 μL of DMEM containing either 10 mM D-glucose (#G8270, Sigma-Aldrich - for glucose consumption and lactate secretion) or 10 mM sodium lactate (for lactate consumption) and supplemented with 2 mM L-glutamine and 10 % dialyzed FBS (#F0392, Sigma-Aldrich). Initial concentrations of glucose and lactate in the experimental medium were also assessed by including control wells containing only cell culture medium (no cells) on each plate. After incubation (from 24 h to 7 days), extracellular media were collected and deproteinized by centrifugation (15 min, 10,000 rpm, 4 °C) in 10 kDa cut-off filter tubes (VWR). Glucose and lactate concentrations were measured in the samples (50 μL) by using enzymatic assays (CMA Microdialysis AB) and an ISCUSflex microdialysis analyzer (Aurora Borealis). Data analysis was done by calculating the difference in glucose and lactate concentrations between the control wells and the experimental wells. Data were then normalized by the protein content in each well and expressed in μmol/hr/mg protein.

2.8. Seahorse analysis

Oxygen consumption rate (OCR) and extracellular acidification rate (ECAR) were measured by using the Seahorse XFe96 plate reader. All assays were carried out using a seeding density of 30,000 cells/well in non-buffered DMEM, adjusted at pH 7.4 and supplemented with specified metabolic substrates. Mitochondrial respiration and glycolytic capacities were assessed by using the XF Cell Mito Stress Test and XF Glycolysis Stress Test, respectively, according to manufacturer's recommendations. Briefly, mitochondrial function parameters (i.e. basal and maximal respirations and ATP production-linked OCR) were evaluated in a DMEM medium containing 10 mM glucose and 2 mM glutamine and after sequential treatment with 1 μM oligomycin, 1 μM carbonyl cyanide-4 (trifluoromethoxy)phenylhydrazone (FCCP) and 0.5 μM rotenone/antimycin A. Lactate-dependent OCR was evaluated upon cell incubation in a medium containing only 10 mM lactate (in absence of glucose and glutamine). Glycolytic function (i.e. basal and maximal glycolytic capacities) was assessed in a DMEM medium containing 2 mM glutamine and after sequential treatment with 10 mM glucose, 1 μM oligomycin and 50 mM 2-DG. Glucose-dependent ECAR was calculated by comparing the values before and after addition of the substrate. Data were normalized by the protein content in each well and expressed in mpH/min/μg protein (ECAR) or pmoles/min/μg protein (OCR).

2.9. Untargeted metabolomics

Cancer cells were seeded (3 × 10^6 cells/dish; 3 dishes/condition) in 60-mm dishes in routine culture medium for 72 h (with medium renewal after 48 h). Medium was then removed, and cells were washed with ice-cold PBS. Dishes were kept from this step on dry ice. Ice-cold methanol 80 % (v/v) was added to each dish (4 mL/dish) and incubated for 20 min at –80 °C. Cells were scraped and transferred to 5 mL Eppendorf tubes pre-cooled in dry ice. Metabolomics standard mix 1 (#MSK-MET1-1; Cambridge Isotope Laboratories), used as an internal standard for untargeted metabolomics, was added to each sample (1.2 μL/sample) which were then directly stored at −80 °C until processing. For further homogenization, zirconia/glass beads (1.0 mm; Biospec Products) were added to the quenched cell suspension and samples were processed on dry ice via a bead beater (FastPrep-24; MP Biomedicals) at 6.0 m/s (3 × 30 s, 5 min pause time). After incubation at −80 °C for 1 h, samples were centrifuged (10 min at 15,000×*g*, 4 °C) and supernatants (1.2 mL cell lysates) were transferred to fresh tubes and dried under a stream of nitrogen. Dried samples were reconstituted in 80 μL acetonitrile:methanol: water (2:2:1, v/v), vortexed for 5 min, centrifuged, and transferred to analytical glass vials. LC-MS grade water, acetonitrile and methanol were obtained from Th. Geyer (Germany). The LC-MS/MS analysis was initiated within 1 h after the completion of the sample preparation.

LC-MS/MS analysis was performed on a Vanquish UHPLC system coupled to an Orbitrap Exploris 240 high-resolution mass spectrometer (Thermo Fisher Scientific) in negative ESI (electrospray ionization) mode. Chromatographic separation was carried out on an Atlantis Premier BEH *Z*-HILIC column (Waters; 2.1 mm × 100 mm, 1.7 μm) at a flow rate of 0.25 mL/min. The mobile phase consisted of water:acetonitrile (9:1, v/v; mobile phase A) and acetonitrile:water (9:1, v/v; mobile phase B), which were modified with a total buffer concentration of 10 mM ammonium acetate (negative mode) and 10 mM ammonium formate (positive mode), respectively. The aqueous portion of each mobile phase was pH-adjusted (negative mode: pH 9.0 via addition of ammonium hydroxide; positive mode: pH 3.0 via addition of formic acid). High-purity ammonium acetate, ammonium formate, formic acid and ammonium hydroxide were purchased from Merck. The following gradient (20 min total run time including re-equilibration) was applied (time [min]/%B): 0/95, 2/95, 14.5/60, 16/60, 16.5/95, 20/95. Column temperature was maintained at 40 °C, the autosampler was set to 4 °C and sample injection volume was 5 μL. Analytes were recorded via a full scan with a mass resolving power of 120,000 over a mass range from 60

to 900 *m/z* (scan time: 100 m s, RF lens: 70 %). To obtain MS/MS fragment spectra, data-dependent acquisition was carried out (resolving power: 15,000; scan time: 22 m s; stepped collision energies [%]: 30/50/70; cycle time: 900 m s). Ion source parameters were set to the following values: spray voltage: 4100 V (positive mode)/−3500 V (negative mode), sheath gas: 30 psi, auxiliary gas: 5 psi, sweep gas: 0 psi, ion transfer tube temperature: 350 °C, vaporizer temperature: 300 °C.

All experimental samples were measured in a randomized manner. Pooled quality control (QC) samples were prepared by mixing equal aliquots from each processed sample. Multiple QCs were injected at the beginning of the analysis in order to equilibrate the analytical system. A QC sample was analyzed after every 5th experimental sample to monitor instrument performance throughout the sequence. For determination of background signals and subsequent background subtraction, an additional processed blank sample was recorded. Data was processed using MS-DIAL [22] and raw peak intensity data was exported. Feature identification was based on accurate mass, isotope pattern, MS/MS fragment scoring and retention time matching to an in-house library. Normalization of the analyzed metabolites was performed on the cell number counted at the moment of the collection of the samples. Metabolites detected in less than 20 % of samples were filtered out. Missing values for the remaining metabolites were imputed using random draws from a Gaussian distribution centered at a minimal value with the imputeLCMD v.2.1 Bioconductor package. Differential expression analysis was performed using limma v.3.54.1 Bioconductor package to obtain fold-change and p-values for each metabolite. *P*-values were adjusted for multiple testing using the Benjamini-Hochberg procedure to control the False Discovery Rate (FDR). Metabolites with an FDR <0.05 and a fold-change greater than 2 were considered modulated. Over-representation analysis (ORA) based on hypergeometric test was conducted from the resulting list of modulated metabolites on the Kyoto Encyclopedia of Gene and Genomes (KEGG) database using fgsea v.1.24.0 Bioconductor package.

2.10. ^{13}C-based metabolic tracing

Cancer cells were seeded (250.000 cells/well; 3 wells/condition) in 6-well plates in routine culture medium for 24 h. The day after, the medium was removed and replaced with culture medium (2 mL/well) containing 10 mM U–^{13}C glucose (#CIL-CLM-1396-2, LGC Standards) and 2 mM unlabeled glutamine for 24 h as well. Medium was then removed, and cells were washed with ice-cold NaCl 0.9 % solution before addition of extraction buffer (300 μL methanol/well) and incubation for 2–3 min on ice. Cells were then harvested using cell scraper and extraction mix was transferred to a new microtube before centrifugation (15.000 rpm for 15 min at 4 °C). Finally, 250 μL of the supernatant (which contains intracellular metabolites) were transferred into a new microtube and stored at −80 °C until mass spectrometry analysis.

Each sample (10 μL) was loaded into a Dionex UltiMate 3000 LC System (Thermo Fisher Scientific) equipped with a C-18 column (Acquity UPLC –HSS T3 1.8 μm; 2.1 × 150 mm, Waters) coupled to a Q Exactive Orbitrap mass spectrometer (Thermo Fisher Scientific) operating in negative ion mode. A step gradient was carried out using solvent A (10 mM TBA and 15 mM acetic acid) and solvent B (100 % methanol). The gradient started with 5 % of solvent B and 95 % solvent A and remained at 5 % B until 2 min post injection. A linear gradient to 37 % B was carried out until 7 min and increased to 41 % until 14 min. Between 14 and 26 min, the gradient increased to 95 % of B and remained at 95 % B for 4 min. At 30 min the gradient returned to 5 % B. The chromatography was stopped at 40 min. The flow was kept constant at 0.25 mL/min and the column was placed at 40 °C throughout the analysis. The MS operated in full scan mode (*m/z* range: [70.0000–1050.0000]) using a spray voltage of 4.80 kV, capillary temperature of 300 °C, sheath gas at 40.0, auxiliary gas at 10.0. The AGC target was set at 3.0 E+006 using a resolution of 140,000, with a maximum IT fill time of 512 m s. Data collection was performed using the Xcalibur software (Thermo Fisher Scientific). Data analyses were performed by integrating the peak areas (El-MAVEN – Polly - Elucidata).

2.11. Statistical analysis

Statistical analyses were performed through GraphPad Prism 10 by using Student's t-test, one-way or two-way ANOVA with Tukey's multiple comparison test when appropriate. Statistical significance is indicated in the figures as follows: $*p < 0.05$; $**p < 0.01$; $***p < 0.001$; ns, not significant.

2.12. Data and material availability

Data from RNA-sequencing analysis, generated during this study, are available at GEO: GSE262796. All unique reagents generated in this study will be made available on request by Prof. Cyril Corbet (cyril.corbet@uclouvain.be) with a completed material transfer agreement (MTA).

3. Results

3.1. Acquired resistance to anti-EGFR therapy is associated with abundance changes for intracellular metabolite in CRC cells

To study the metabolic adaptation of CRC cells upon acquired resistance to cetuximab treatment, we first used two human colon cancer cell lines LIM1215 and DiFi, initially cetuximab-sensitive (denoted as –S), and for which populations with acquired resistance (-R1 and -R2) had been previously established upon chronic exposure for several months with the drug [17] (Fig. 1A). While DiFi-R cells harbored *EGFR* gene copy number reduction and *KRAS* gene amplification, LIM1215-R cells were reported to display *KRAS* activating mutations (p.G12R and p.G13D for LIM1215-R1 and -R2, respectively) [17] (Fig. S1A). In both DiFi-R and LIM1215-R cells, genomic changes (i.e. amplification or mutations, respectively) in *KRAS* were accompanied by increased basal activation of MAPK signaling pathway (Fig. S1B). Untargeted metabolomic analysis was first carried out to reveal abundance changes for intracellular metabolites between parental and cetuximab-resistant LIM1215 and DiFi cells (Fig. 1B). Only 4 metabolites were found to be commonly downregulated in LIM1215-R1 and -R2 cell populations (vs LIM1215-S cells), while 42 metabolites were consistently upregulated in both cetuximab-resistant LIM1215 cells (Fig. 1C–D and Tables S1–2). Metabolic alterations were even scarcer in DiFi-R cells, with only 16 metabolites being commonly downregulated (and none being upregulated) in both R1 and R2 cell populations, respectively (Figs. S1C–D and Tables S3–4). Surprisingly, we could not identify any metabolite commonly regulated in the four different cetuximab-resistant CRC cell models. Instead, we showed a greater similarity of the metabolic profiles between R1 and R2 populations derived from the same parental cell line (i.e. DiFi or LIM1215), as revealed by principal component analysis (Fig. S1E). Pathway enrichment analysis documented the distinct metabolic rewiring upon acquired resistance to cetuximab in our CRC cell models with glycolysis/gluconeogenesis as the most differentially enriched metabolic process in cetuximab-resistant LIM1215 cells (Fig. 1E), while amino acid metabolism was noticeably enriched in DiFi-R cells (Fig. S1F).

3.2. Glycolysis is upregulated in KRAS-mutant cetuximab-resistant CRC cells

Since cetuximab was shown to exert its antitumor activity, at least partly, via the inhibition of HIF1-mediated glycolysis in cancer cells [23–25], we first explored potential changes in glucose metabolism. We found that intracellular abundance of glycolytic intermediates (i.e. glyceraldehyde-3-phosphate (G3P), pyruvate and lactate) was higher in LIM1215-R1 and -R2 (vs –S cells), but not in cetuximab-resistant DiFi

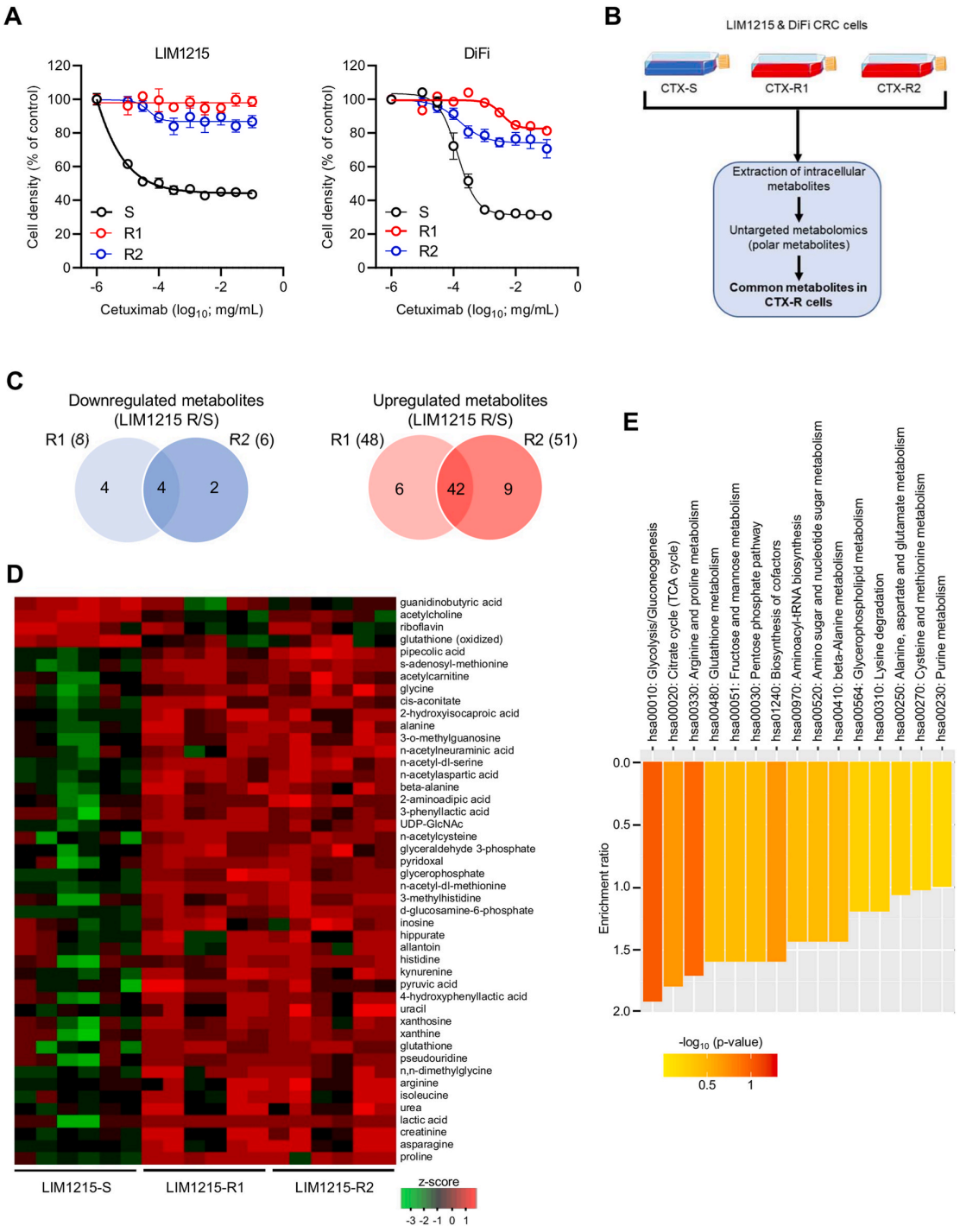

Fig. 1. Metabolism is rewired in CRC cells upon acquired resistance to *anti*-EGFR therapy. (**A**) Viability of cetuximab-sensitive (S) and resistant (R1 and R2) LIM1215 and DiFi cells after treatment with increasing concentrations of cetuximab for 72 h. (**B**) Experimental workflow for the metabolomic analysis carried out in cetuximab-sensitive (S) and resistant (R1 and R2) LIM1215 and DiFi cells. (**C**) Venn diagrams depicting the number of metabolites commonly downregulated (left panel) or upregulated (right panel) in both cetuximab-resistant (R1 and R2) LIM1215 cell populations (vs LIM1215-S cells). (**D-E**) Heatmap of the commonly regulated metabolites (**D**) and pathways significantly enriched from overrepresentation analysis (**E**) in both cetuximab-resistant (R1 and R2) LIM1215 cell populations (vs LIM1215-S cells). Data are plotted as the means ± SEM from n = 3 cultures, performed each time with ≥3 technical replicates (**A**). Metabolomics data (**C-E**) were acquired from 3 independent cell cultures with 2 technical replicates.

cells (Fig. 2A and Fig. S2A). Glucose consumption, lactate secretion and lactate/glucose ratio were also increased in cetuximab-resistant LIM1215 cells, while no change was observed in DiFi cells (Fig. 2B–C and Fig. S2B). Interestingly, by using an additional cetuximab-resistant OXCO2-R6 cell model (Fig. S2C), that harbors a KRAS activating mutation (p.G13D like LIM1215-R2 cells), we also observed an increased glycolytic activity, in comparison to parental cetuximab-sensitive cell counterparts (Figs. S2D–E). Accordingly, glucose-induced and maximal extracellular acidification rates (ECAR) were upregulated upon acquired resistance to cetuximab in LIM1215 cells, while being not affected in DiFi cells (Fig. 2D–F and Fig. S2F). To better understand the intracellular fate of glucose (e.g. through glycolysis or serine biosynthesis pathway), cetuximab-sensitive and -resistant LIM1215 and DiFi cells were incubated for 24 h with a uniformly labelled ^{13}C-glucose tracer before mass spectrometry analysis (Fig. 2G). This revealed a significant increase of labeling in glycolysis intermediates, including hexose-phosphate (i.e. glucose-6-phosphate and/or fructose-6-phosphate), G3P, pyruvate and lactate in cetuximab-resistant LIM1215 cells, while labeling was not or barely changed in DiFi-R cell populations (Fig. 2H–J and S2G-I). We also observed a greater contribution for glucose in amino acid labeling (i.e. serine, glycine and alanine) in LIM1215-R cells, but not in DiFi-R cells (Fig. 2K-L and S2J-K). Importantly, ^{13}C-glucose tracing experiments showed an increased labeling of tricarboxylic acid (TCA) cycle metabolic intermediates, including malate, fumarate and aspartate, through the conversion of pyruvate either into acetyl-CoA (via pyruvate dehydrogenase (PDH) activity giving rise to m+2 labeling) or into malate (via pyruvate carboxylase (PC) activity leading to m+3 labeling) in cetuximab-resistant LIM1215 cells, but not in DiFi cells (Fig. 3A–C and Fig. S3A-B). Nevertheless, Seahorse-based assessment of oxygen consumption rates (OCR) did not reveal any major change of mitochondrial respiration when CRC cells were cultured in presence of glucose (and glutamine) (Fig. 3D and Fig. S3C). Instead, we reported a decrease of basal, maximal and ATP-linked respiration capacities in some cetuximab-resistant CRC cells (vs cetuximab-sensitive cells) (Fig. 3E–G). Altogether these data suggest a major role for glucose metabolism to support both bioenergetic and biosynthetic needs in *KRAS*-mutant cetuximab-resistant CRC cells with an enhanced glycolytic activity leading to lactate production.

3.3. *KRAS-mutant cetuximab-resistant CRC cells can recycle glycolysis-derived lactate to sustain growth in glucose-limited conditions*

In order to have a more dynamic view of glucose utilization and lactate release over the time in the different CRC cell populations, we assessed glucose and lactate extracellular levels for 7 days upon cell seeding in a medium initially containing 10 mM glucose. Importantly, we did not refresh the medium during this period of time and we used 10 % dialyzed fetal bovine serum to prevent the presence of any trace of glutamine or lactate at the onset. As expected, based on our previous results (see Fig. 2B–C), we showed that both LIM1215-R1 and R2 cell populations had a greater glycolysis activity (vs LIM1215-S cells and DiFi cells), with glucose being fully consumed and lactate levels peaking after 2 days of incubation (Fig. 4A). Interestingly, we observed that lactate levels progressively decreased when cells were maintained in glucose-deprived conditions, thereby suggesting that the cells had the capacity to take up lactate and use it as an energetic fuel. Indeed, when determining the lactate recycling capacity in CRC cells, based on the slopes of the curves for lactate levels between days 3 and 7, we showed that cetuximab-resistant LIM1215 cells had a greater capacity to import glycolysis-derived lactate when facing glucose deprivation (Fig. 4B). Of note, although lactate levels were also decreased between days 3 and 7 with DiFi cells, we did not observe any difference for lactate utilization between cetuximab-sensitive and -resistant cells (Fig. 4A–B). To further prove the ability of CRC cells to take up and use exogenous lactate as an energetic fuel, we first incubated cells in medium containing only lactate (i.e. instead of glucose). We validated a higher lactate consumption in cetuximab-resistant LIM1215 and OXCO2 cells (vs parental cells) (Fig. 4C and Fig. S4A), and this was associated with an increased lactate-dependent mitochondrial respiration, as revealed by Seahorse-based bioenergetic analysis (Fig. 4D). Finally, we showed that cetuximab-resistant LIM1215 and OXCO2 cells were more prone to grow in a lactate-containing medium for 72 h, in comparison to cetuximab-sensitive cell counterparts (Fig. 4E and Fig. S4B), further proving that increased metabolic flexibility (i.e. capacity to use different nutrients), here exemplified by a capacity to use either glucose or lactate, was a phenotypic advantage for *KRAS*-mutant cetuximab-resistant CRC cells to sustain their growth despite changes in nutrient availability.

3.4. *MCT1 overexpression supports lactate utilization in KRAS-mutant cetuximab-resistant CRC cells*

We then carried out a bulk RNA-sequencing analysis with the aim to reveal transcriptomic changes in cetuximab-resistant CRC cells and identify potential candidates supporting the metabolic reprogramming towards glycolysis. This allowed us to document expression changes for hundreds of genes between cetuximab-resistant and -sensitive DiFi and LIM1215 cells (Tables S5–8), and a closer look at glycolysis-related genes highlighted *HK2*, *SLC16A1* and *ENO3* as the only three genes consistently upregulated in both cetuximab-resistant LIM1215 cell populations (Fig. 5A). While *HK2* and *ENO3* genes encode enzymes (hexokinase 2 and enolase 3, respectively) that directly participate to the glycolytic pathway, *SLC16A1* is the gene for monocarboxylate transporter 1 (MCT1) mostly involved in lactate influx in several cancer types [26], making the latter a potential key actor for the metabolic reprogramming in cetuximab-resistant CRC cells. MCT1 upregulation was found in LIM1215-R cell populations, but not in DiFi-R cells, both at mRNA and protein levels (Fig. 5B–D), and it was also observed in OXCO2-R6 cells (Fig. 5C and Fig. S4C), thereby suggesting that increased MCT1 protein levels were specific to *KRAS*-mutant cetuximab-resistant CRC cells. Even more importantly, when treating the cells with AR-C155858, a specific MCT1 inhibitor [27], as lactate levels peak (i.e. 3 days post-incubation in a glucose-containing medium), we showed that lactate recycling capacity was strongly impaired in cetuximab-resistant LIM1215 cells, but not in DiFi cells (Fig. 5E–F and S4D-E). A similar decrease of lactate consumption (Fig. 5G and Fig. S4F) and oxidation (Fig. 5H) was observed upon AR-C155858 treatment when cetuximab-resistant LIM1215 and OXCO2 cells were incubated in a lactate-containing medium, thereby validating the straightforward contribution of MCT1 for lactate utilization in *KRAS*-mutant cetuximab-resistant CRC cells.

3.5. *Pharmacological inhibition of MCT1 induces detrimental effects in KRAS-mutant cetuximab-resistant CRC cells*

Finally, we investigated whether, and if so how, MCT1 upregulation could be exploited, from a therapeutic point of view, to kill specifically CRC cells upon acquired resistance to *anti*-EGFR therapy. First, we showed that preventing the use of lactate as energetic fuel by inhibiting MCT1 with AR-C155858, when glucose was limited (i.e. 3 days post-seeding in a glucose-containing medium), significantly delayed the growth of cetuximab-resistant LIM1215 cells, but not for cetuximab-sensitive cells (Fig. 6A–B). Similarly, pharmacological inhibition of MCT1 induced specific growth-inhibitory effects in cetuximab-resistant LIM1215 and OXCO2 cells, but not in DiFi cells, upon incubation in a lactate-containing medium (Fig. 6C and Fig. S5A-B). Importantly, we showed that treatment with AR-C155858 was able to resensitize LIM1215-R and OXCO2-R cell populations to cetuximab (Fig. 6D and Fig. S5C). As another approach, since MCT1 was shown to be the main entry path for 3-bromopyruvate (3-BrPA), a potent metabolic inhibitor [28,29], we also tested whether an upregulation of the transporter could make the cetuximab-resistant cells more vulnerable to this inhibitor. Indeed, we observed a greater reduction of viability for

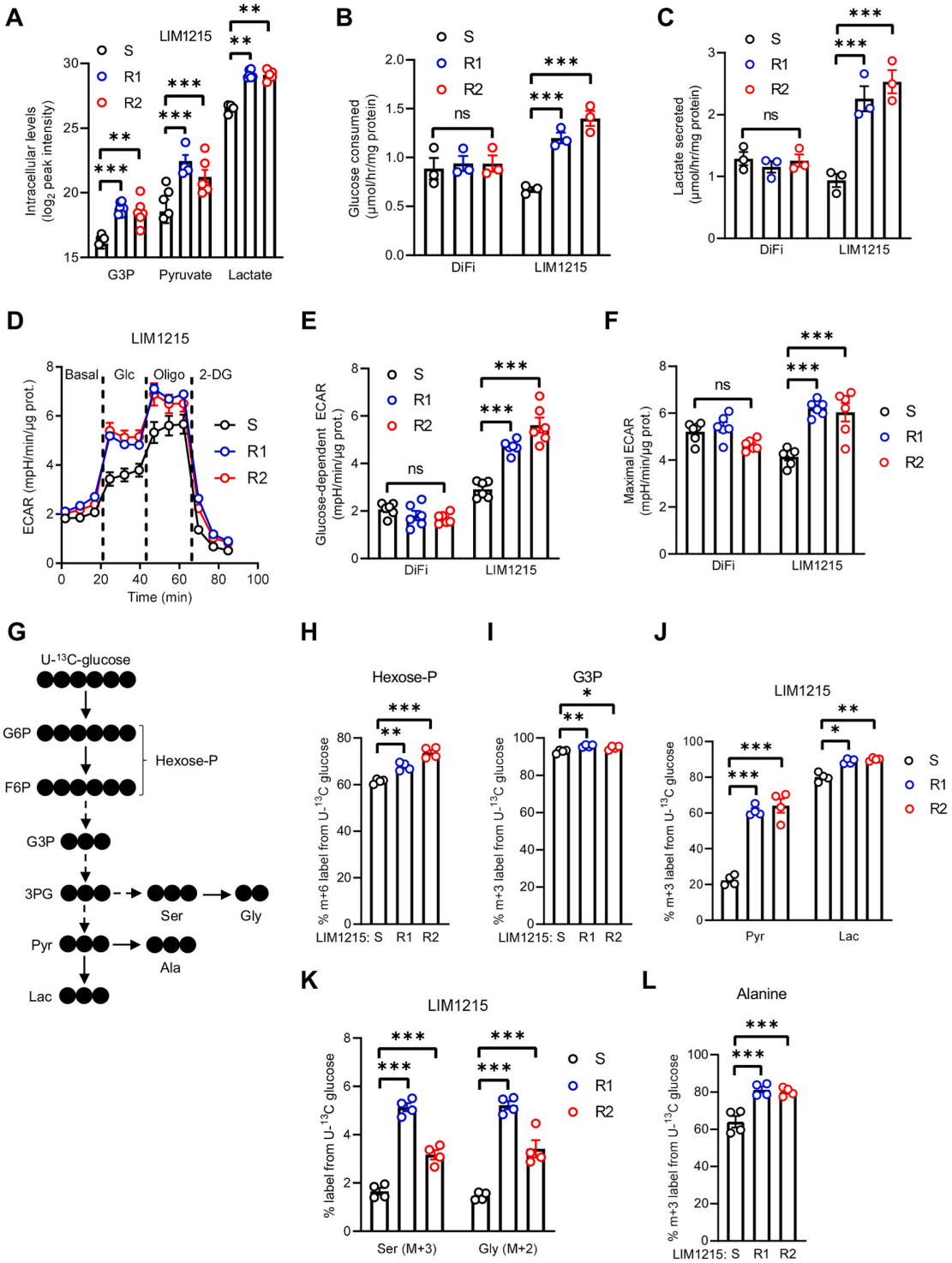

Fig. 2. Glycolytic activity is increased in *KRAS*-mutant cetuximab-resistant LIM1215 cells. (**A**) Intracellular levels of glyceraldehyde-3-phosphate (G3P), pyruvate and lactate in cetuximab-sensitive (S) and resistant (R1 and R2) LIM1215 cells. (**B–C**) Glucose consumption (**B**) and lactate secretion (**C**) in cetuximab-sensitive (S) and resistant (R1 and R2) DiFi and LIM1215 cells. (**D**) Extracellular acidification rates (ECAR) in cetuximab-sensitive (S) and -resistant (R1 and R2) LIM1215 cells upon sequential treatment with 10 mM glucose, 1 µM oligomycin and 50 mM 2-deoxyglucose (2-DG). (**E-F**) Glucose-dependent (**E**) and maximal ECAR (**F**) in cetuximab-sensitive (S) and resistant (R1 and R2) DiFi and LIM1215 cells. (**G**) Carbon atom transition map depicting labeling of glycolytic metabolites from [U–$^{13}C_6$]glucose. (**H-L**) Relative abundance of glycolysis-specific mass isotopomers for hexose-phosphate (**H**), G3P (**I**), pyruvate and lactate (**J**), serine and glycine (**K**) and alanine (**L**) in cetuximab-sensitive and -resistant (R1 and R2) LIM1215 cells cultured for 24 h in the presence of 10 mM [U–$^{13}C_6$]glucose. Data are plotted as the means ± SEM from n = 3 cultures, performed each time with ≥3 technical replicates (**A-F** and **H-L**). Significance was determined by one-way ANOVA (**H–I** and **L**) or two-way ANOVA (**A-C**, **E-F** and **J-K**) with Tukey's multiple comparison test. *p < 0.05; **p < 0.01; ***p < 0.001; ns, not significant.

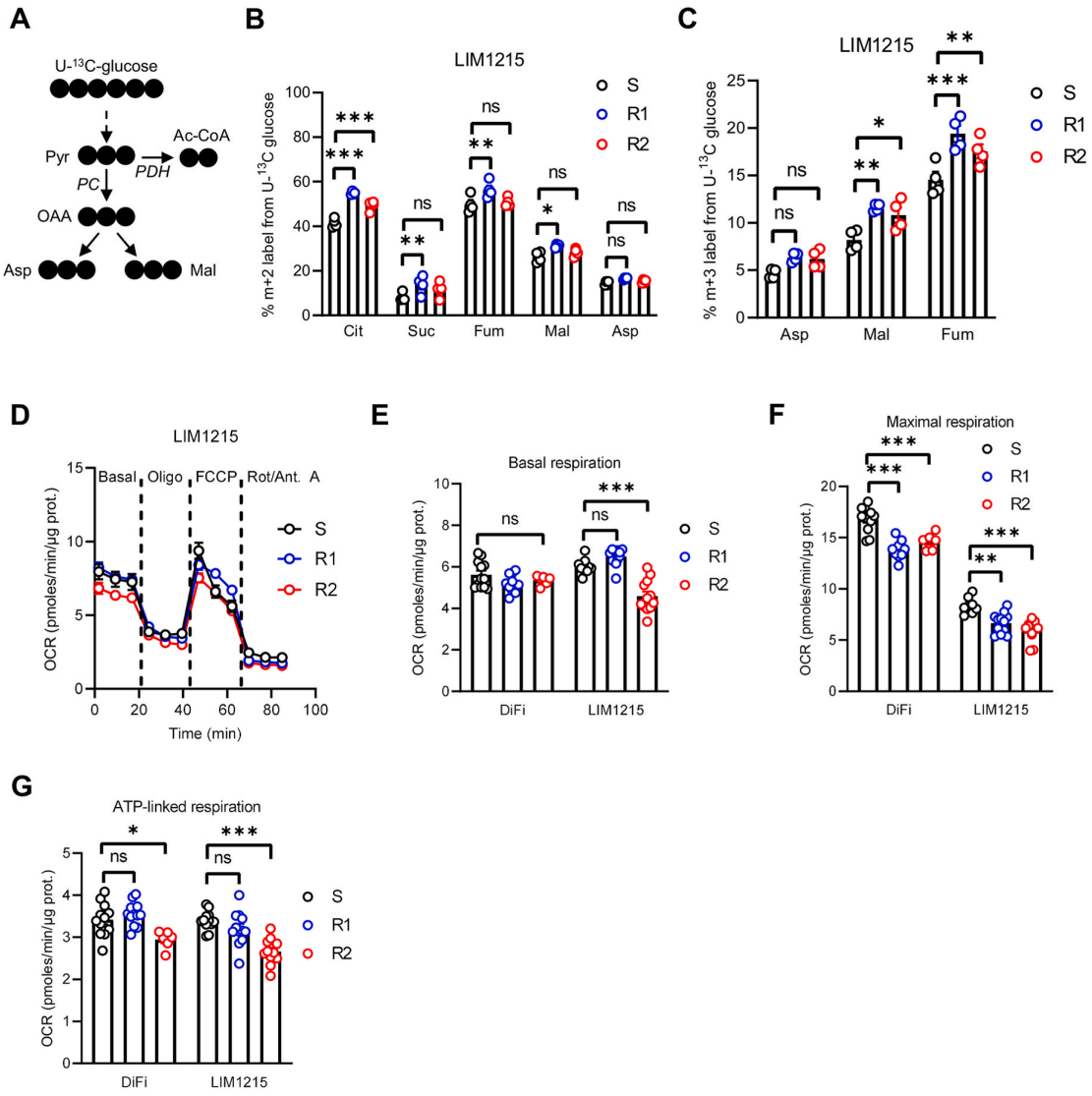

Fig. 3. Mitochondrial respiration is barely affected in CRC cells upon acquired resistance to cetuximab. (**A**) Carbon atom transition map depicting labeling of TCA cycle intermediates from [U–$^{13}C_6$]glucose-derived pyruvate upon activity of pyruvate dehydrogenase (PDH) or pyruvate carboxylase (PC). (**B–C**) Relative abundance of specific mass isotopomers for TCA cycle intermediates upon activity of PDH (**B**) or PC (**C**) in cetuximab-sensitive and -resistant (R1 and R2) LIM1215 cells cultured for 24 h in the presence of 10 mM [U–$^{13}C_6$]glucose. (**D**) Oxygen consumption rates (OCR) in cetuximab-sensitive (S) and -resistant (R1 and R2) LIM1215 cells upon sequential treatment with 1 µM oligomycin, 1 µM FCCP and 0.5 µM rotenone/antimycin A. (**E-G**) Basal (**E**), maximal (**F**) and ATP-linked (**G**) OCR in cetuximab-sensitive (S) and -resistant (R1 and R2) DiFi and LIM1215 cells. Data are plotted as the means ± SEM from n = 3 cultures, performed each time with ≥3 technical replicates (**B-G**). Significance was determined by two-way ANOVA (**B–C**, and **E-G**) with Tukey's multiple comparison test. *p < 0.05; **p < 0.01; ***p < 0.001; ns, not significant.

cetuximab-resistant LIM1215 cells (vs LIM1215-S cells) upon treatment with 50 µM 3-BrPA for 72 h (Fig. 6E).

Finally, since lactate metabolism has already been reported to support pleiotropic pro-tumorigenic effects in cancer cells [30], we also evaluated the potential importance of MCT1-dependent lactate utilization on *KRAS*-mutant cetuximab-resistant CRC cell phenotype, by carrying out *in vitro* migration assays in presence or not of the MCT1 inhibitor AR-C155858. We reported that LIM1215-R1 and -R2 cells were not more migratory than parental LIM1215-S cells and that MCT1 inhibition did not modify the migration capacity of the different cell populations (Fig. S5D). Surprisingly, we observed that AR-C155858 treatment induced a significant increase of migration for both DiFi-R1 and -R2 populations while they were initially less migratory than DiFi-S cells (Fig. S5E). Finally, we showed that OXCO2-R6 cells were more migratory than OXCO2-S cells but this pro-migratory capacity was not altered upon treatment with AR-C155858 (Fig. S5F). Overall, these data do not seem to be in favor of a major role of lactate metabolism for cell migration in cetuximab-resistant CRC cells. We then carried out an *in vivo* experiment with tumor xenografts from LIM1215-S or -R1 cells treated or not with AR-C155858. We observed that tumor growth for LIM1215-R1 cells was reduced after 4 weeks of treatment with 3 mg/kg AR-C155858 (Fig. 6F–H) while growth of LIM1215-S tumors was not changed (Figs. S5G–I). These data validate our *in vitro* data about the specific growth-inhibitory effect of MCT1 inhibition in cetuximab-resistant LIM1215 cells (vs cetuximab-sensitive LIM1215 cells). Altogether, these data show that MCT1 upregulation and subsequent enhanced lactate metabolism might be therapeutically exploited by different means to reduce growth of *KRAS*-mutant CRC cells upon

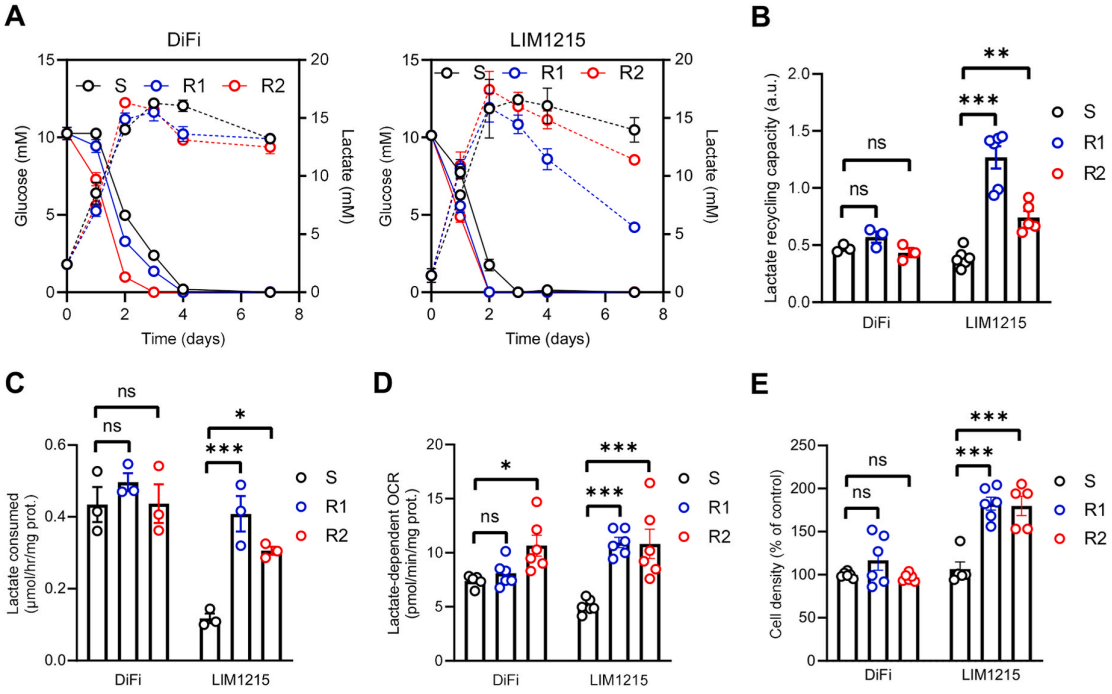

Fig. 4. *KRAS*-mutant cetuximab-resistant CRC cells recycle lactate to sustain their proliferative capacity. (**A**) Evolution of glucose and lactate concentrations (solid and dashed lines, respectively) for 7 days in media from cetuximab-sensitive and -resistant (R1 and R2) DiFi and LIM1215 cells initially incubated in a medium containing 10 mM glucose. (**B**) Lactate recycling capacity in cetuximab-sensitive and -resistant (R1 and R2) DiFi and LIM1215 cells. (***C*-E**) Lactate consumption (**C**), lactate-dependent OCR (**D**) and growth in a lactate-containing medium for 72 h (**E**) for cetuximab-sensitive and -resistant (R1 and R2) DiFi and LIM1215 cells. Data are plotted as the means ± SEM from n = 3 cultures, performed each time with ≥3 technical replicates (**A-E**). Significance was determined by two-way ANOVA (**B-E**) with Tukey's multiple comparison test. *p < 0.05; **p < 0.01; ***p < 0.001; ns, not significant.

acquired resistance to cetuximab.

4. Discussion

In the current era of precision oncology, resistance to targeted therapies remains a critical hurdle in our ambition for curative cancer treatments [31]. For instance, the clinical efficacy of *anti*-EGFR monoclonal antibodies in mCRC patients is strongly limited by the development of acquired drug resistance after an initial tumor response. Indeed, while cetuximab or panitumumab can induce a tumor regression, the clinical response is frequently incomplete and long-term clinical relapse inevitably ensues due to the emergence of therapy-resistant cells [32]. Over the years, several mechanisms supporting acquired resistance to *anti*-EGFR therapy in mCRC have been identified, including mainly genetic alterations [33,34] but also non-genetic changes such as overexpression of long non-coding RNA [35]. Nevertheless, it has not modified yet the routine clinical care of mCRC patients, thereby highlighting the need for a better characterization of cetuximab-resistant mCRC and for the discovery of new actionable targets to therapeutically exploit resistance-associated phenotypic changes. In this study, we aimed to tackle the issue of acquired resistance to cetuximab in CRC through a specific metabolic angle. Indeed, metabolic rewiring has emerged as a critical mechanism for the adaptation and resistance to anticancer therapies, including targeted agents, thereby creating a new field of investigation for the development of novel anticancer agents with the potential to overcome therapeutic resistance [36,37].

Here, we have shown that acquired resistance to cetuximab in CRC cells is associated with several metabolic alterations, including changes of intracellular abundance for amino acids as well as for glucose and glutamine metabolism intermediates. Remarkably, our analyses have revealed that cetuximab-resistant LIM1215-R1 and -R2 cell populations, harboring distinct resistance-causing KRAS-activating mutations (p.G12R and p.G13D, respectively), exhibit common metabolic phenotypes, with enhanced glucose consumption and lactate secretion. More specifically, we have reported the ability of cetuximab-resistant CRC cells to recycle glycolysis-derived lactate to sustain their growth capacity. Our observations are reminiscent of previous studies that showed a major role for lactate metabolism to support adaptive resistance to various targeted therapies, including MET and EGFR tyrosine kinase inhibitors in non-small cell lung cancers and breast cancers [38], PI3K/mTOR inhibitors in breast cancers [39], pan-Akt inhibitor (uprosertib) in colon cancers [40], and anti-angiogenic therapies in breast cancers [41]. More recently, Monteith and colleagues observed that acute myeloid leukemia cells could resist to BET inhibitors by utilizing lactate as a metabolic bypass to fuel mitochondrial respiration and maintain cellular viability [42]. These studies also reported the contribution of MCT1 as the main lactate transporter in therapy-resistant cancer cells, with genetic invalidation or pharmacological inhibition of MCT1 being able to revert the phenotype and sensitize cells to therapy. In our study, we have shown that MCT1-dependent lactate utilization is restricted to cetuximab-resistant CRC cells carrying *KRAS* gene mutations. This increased metabolic flexibility may mirror the need for highly proliferating cells to metabolically switch towards the use of alternative energetic substrates, including lactate, when facing restricted availability of glucose, as already reported elsewhere [43]. In the same line, lactate metabolism has also been reported to be important in lung adenocarcinomas carrying *KRAS* mutations, with expression of lactate dehydrogenase B (mostly catalyzing the conversion of lactate to pyruvate) being associated with a shorter survival for *KRAS*-driven lung adenocarcinoma patients [44]. Further studies are now needed to better understand the molecular mechanisms involved in MCT1 transporter upregulation in *KRAS*-mutant cetuximab-resistant CRC cells. MYC oncoprotein may be a major actor since it has already been described to control transcriptional expression of *SLC16A1*/MCT1 [45] and *MYC*

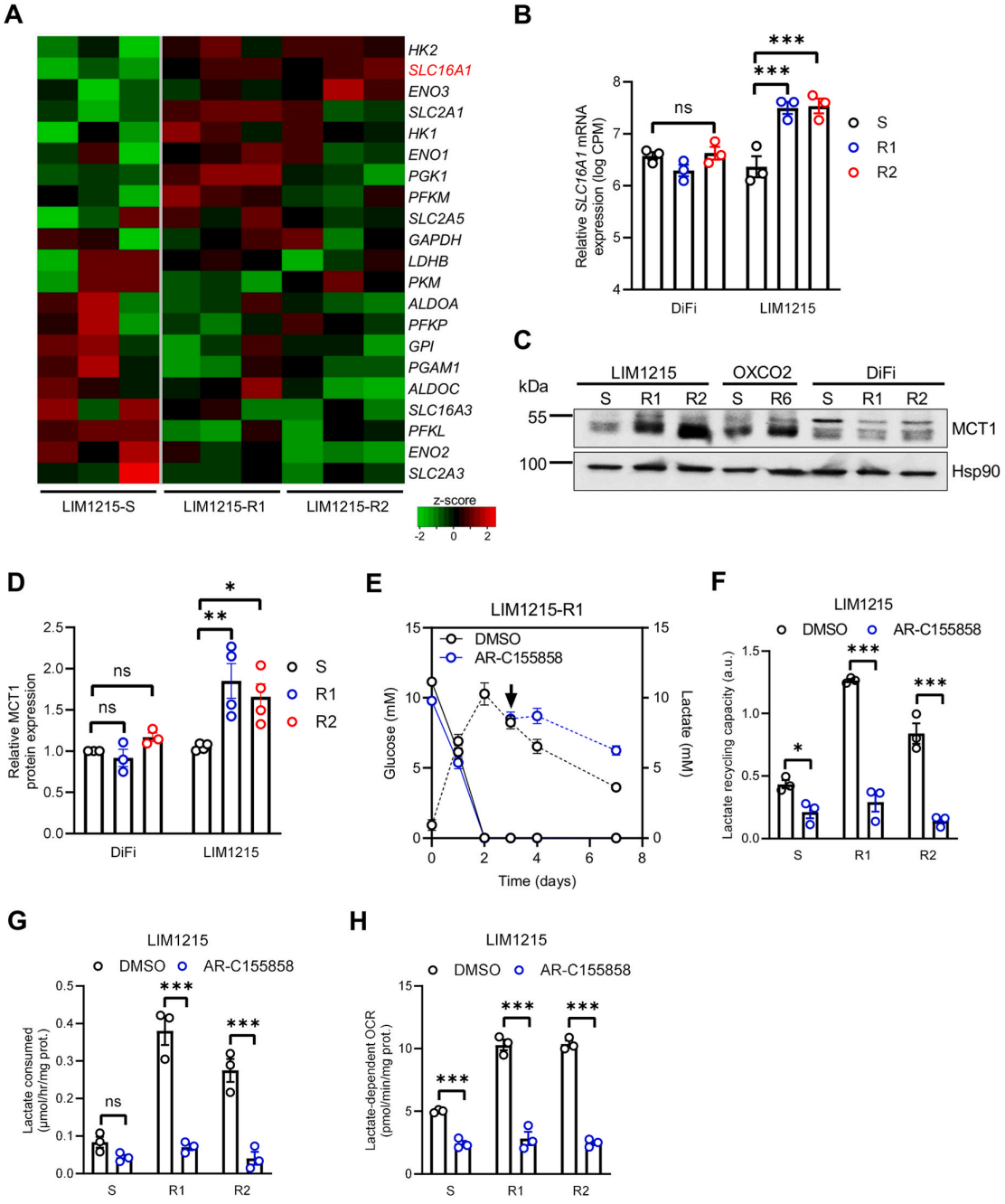

Fig. 5. MCT1 upregulation sustains lactate recycling in *KRAS*-mutant cetuximab-resistant CRC cells. (**A**) Heatmap of glycolysis-related genes in cetuximab-sensitive and -resistant LIM1215 cells. (**B**) mRNA expression levels for *SLC16A1* in cetuximab-sensitive and -resistant (R1 and R2) DiFi and LIM1215 cells. (**C-D**) Representative immunoblotting (**C**) and quantification (**D**) for MCT1 in cetuximab-sensitive and -resistant DiFi, LIM1215 and OXCO2 cells. (**E**) Evolution of glucose and lactate concentrations (solid and dashed lines, respectively) for 7 days in media from cetuximab-resistant (R1) LIM1215 cells initially incubated in a medium containing 10 mM glucose and treated at day 3 (as indicated with an arrow) with 10 µM AR-C155858. (**F**) Lactate recycling capacity in cetuximab-sensitive and -resistant (R1 and R2) LIM1215 cells treated with 10 µM AR-C155858 for 96 h. (**G-H**) Lactate consumption (**G**) and lactate-dependent OCR (**H**) for cetuximab-sensitive and -resistant (R1 and R2) LIM1215 cells treated with 10 µM AR-C155858 for 24 h. Data are plotted as the means ± SEM from n = 3–4 cultures, performed each time with ≥3 technical replicates (**B** and **D-H**). Significance was determined by two-way ANOVA (**B**, **D** and **F–H**) with Tukey's multiple comparison test. *p < 0.05; **p < 0.01; ***p < 0.001; ns, not significant.

gene expression is downstream of RAS signaling, with a constitutive expression of MYC in the presence of oncogenic mutations of *KRAS* [46, 47]. A recent study has also reported the identification and use of a reliable lactate-related gene signature to predict response to anticancer treatments, including immuno- and chemotherapies, and clinical outcomes in patients with CRC [48]. Additionally, although this has not been further explored in our study, our metabolomics analyses also revealed some changes in glutamine/glutamate metabolism, including glutathione synthesis in cetuximab-resistant CRC cells. Glutamine metabolism is well known to be reprogrammed during cancer

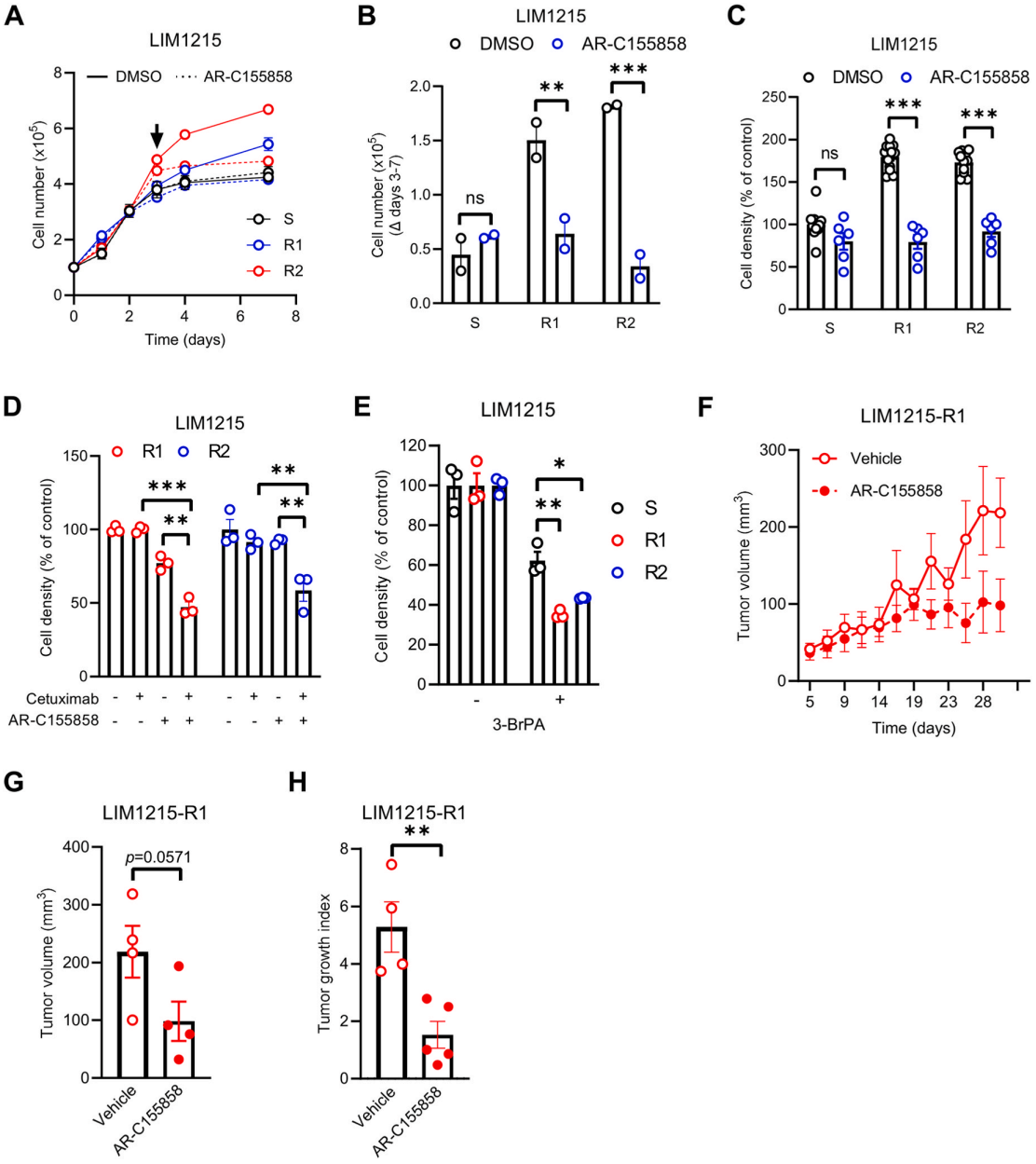

Fig. 6. MCT1 inhibition overcomes acquired resistance to cetuximab in *KRAS*-mutant CRC cells. (**A**) Growth (for 7 days) of cetuximab-resistant (R1) LIM1215 cells initially incubated in a medium containing 10 mM glucose and treated at day 3 (as indicated with an arrow) with 10 μM AR-C155858 or DMSO as vehicle (dashed and solid lines, respectively). (**B**) Cell number differences between days 3 and 7 in the panel A. (**C**) Growth in a lactate-containing medium for cetuximab-sensitive and -resistant (R1 and R2) LIM1215 cells treated or not with 10 μM AR-C155858 for 72 h. (**D**) Growth of cetuximab-resistant (R1 and R2) LIM1215 cells upon treatment with 10 μM AR-C155858 and 25 μg/mL cetuximab in combination or alone for 72 h in routine culture medium. (**E**) Growth of cetuximab-sensitive and -resistant (R1 and R2) LIM1215 cells upon treatment with 50 μM 3-bromopyruvate (3-BrPA) for 72 h in routine culture medium. (**F**) Volume of LIM1215-R1 tumor xenografts in nude mice (n = 4 for each group) daily treated with 3 mg/kg AR-C155858 (or DMSO as vehicle). (**G-H**) Tumor volume (**G**) and tumor growth index (**H**) at day 30 (end point). Data are plotted as the means ± SEM from n = 2–3 cultures, performed each time with ≥3 technical replicates (**A-E**). Significance was determined by two-way ANOVA (**B-E**) with Tukey's multiple comparison test. *p < 0.05; **p < 0.01; ***p < 0.001; ns, not significant.

progression, including escape to conventional treatments, and it has been investigated as a promising target for cancer therapy [49]. A combined treatment with cetuximab and CB-839, a glutaminase inhibitor, has shown its capacity to overcome acquired resistance to *anti*-EGFR antibody in a specific 3D culture of colonies with cystic morphology from the human *RAS/BRAF* wild-type, microsatellite unstable CRC cell line HCA-7 [50]. Moreover, overexpression of the glutamine transporter SLC1A5 has been reported in CRC patients with cetuximab resistance and its inhibition sensitizes CRC cells to *anti*-EGFR therapy [51]. Nevertheless, in the latter study, there was no information about the resistance status (i.e. primary vs secondary) and genetic alterations (if any) associated with the resistance to *anti*-EGFR therapy.

Finally, it remains unclear why, despite *KRAS* gene amplification, lactate metabolism does not change in cetuximab-resistant DiFi cells. As previously reported [17], activation of EGFR downstream signaling pathways is somewhat different in cetuximab-resistant DiFi and

LIM1215 cells, with for instance a decrease of phosphorylated Akt (Ser-473) in DiFi-R1 and -R2 cells (vs DiFi-S cell population) whereas pAkt levels are maintained between all LIM1215 cell populations. On contrary, phosphorylation levels of MEK and Erk1/2 are found to be increased in cetuximab-resistant DiFi cells while being barely affected in cetuximab-resistant LIM1215 cells (vs parental LIM1215 cells). Overall, this will lead to very distinct transcriptional programs in the different cetuximab-resistant CRC cell models, illustrated with the *SLC16A1* gene upregulation only present in cetuximab-resistant LIM1215 cells. Metabolic reprogramming, including changes in lactate metabolism, may be thus seen as a consequence, rather than a cause, of the oncogene-driven acquired resistance to cetuximab in CRC cells.

In conclusion, the diversity of resistance-associated genomic alterations in mCRC patients is still a major limitation for the clinical success of targeted therapies such as *anti*-EGFR mAbs. The current record of therapy failure and clinical relapse also highlights the urgent need to implement fundamental changes in the treatment paradigm of these patients. Adding a new layer of sophistication for precision medicine, by considering the metabolic phenotypes shared by tumors exhibiting therapy resistance, may offer new therapeutic approaches to improve response to targeted therapies and delay or overcome development of secondary resistance mechanisms [52]. Our study paves the way for the development of novel strategies aiming to target lactate metabolism, including MCT1 activity, to improve response to *anti*-EGFR therapy in mCRC patients.

CRediT authorship contribution statement

Elena Richiardone: Writing – original draft, Investigation, Formal analysis, Conceptualization. **Rim Al Roumi:** Investigation, Formal analysis. **Fanny Lardinois:** Investigation. **Maria Virginia Giolito:** Investigation, Formal analysis. **Jérôme Ambroise:** Software, Methodology, Formal analysis, Data curation. **Romain Boidot:** Methodology. **Bernhard Drotleff:** Methodology. **Bart Ghesquière:** Methodology. **Akeila Bellahcène:** Methodology. **Alberto Bardelli:** Resources, Methodology, Funding acquisition. **Sabrina Arena:** Resources, Methodology, Funding acquisition, Formal analysis. **Cyril Corbet:** Writing – original draft, Supervision, Project administration, Funding acquisition, Formal analysis, Conceptualization.

Declaration of competing interest

The authors declare the following financial interests/personal relationships which may be considered as potential competing interests: S. A. reports personal fees from MSD Italia and a patent (international PCT patent application No. WO 2023/199255 and Italian patent application No. 102022000007535) outside the submitted work. A.Ba. reports receipt of grants/research support from Neophore, AstraZeneca and Boehringer Ingelheim and honoraria/consultation fees from Guardant Health and Inivata. A.Ba. is a stock shareholder of Neophore and Kither Biotech. A.Ba. is an advisory board member for Inivata, Neophore, Roche/Genentech. The other authors declare no competing interests.

Acknowledgements

This work was supported by research grants from the Fonds National de la Recherche Scientifique (F.R.S.-FNRS), the Belgian Foundation against Cancer, and the J. Maisin Foundation. The research leading to these results has also received funding from: AIRC under BRIDGE 2022-ID 27321 project (S.A.), MUR Dipartimento di Eccellenza 2023–2027 14586 DIORAMA (S.A.), Finanziamento dell'Unione Europea Next-Generation EU M4 C2 investimento 1.1.- PRIN 2022 PNRR P2022E3BTH (S.A.), Italian Ministry of Health, Ricerca Corrente 2024 (S.A.), AIRC under 5 per Mille 2018 - ID. 21091 program (A.Ba.); International Accelerator Award, ACRCelerate, jointly funded by Cancer Research UK (A26825 and A28223), FC AECC (GEACC18004TAB) and AIRC (22795) (A.Ba.); AIRC under IG 2023 - ID. 28922 project (A.Ba.) and PRIN 2022 - Prot. 2022CHB9BA (A.Ba.). CC is a FNRS Research Associate. ER is a FNRS-FRIA PhD fellow. AB is a FNRS Research Director.

Appendix A. Supplementary data

Supplementary data to this article can be found online at https://doi.org/10.1016/j.canlet.2024.217091.

References

[1] C. Bokemeyer, I. Bondarenko, A. Makhson, J.T. Hartmann, J. Aparicio, F. de Braud, et al., Fluorouracil, leucovorin, and oxaliplatin with and without cetuximab in the first-line treatment of metastatic colorectal cancer, J. Clin. Oncol. 27 (5) (2009) 663–671.
[2] J.Y. Douillard, S. Siena, J. Cassidy, J. Tabernero, R. Burkes, M. Barugel, et al., Randomized, phase III trial of panitumumab with infusional fluorouracil, leucovorin, and oxaliplatin (FOLFOX4) versus FOLFOX4 alone as first-line treatment in patients with previously untreated metastatic colorectal cancer: the PRIME study, J. Clin. Oncol. 28 (31) (2010) 4697–4705.
[3] E. Van Cutsem, C.H. Kohne, E. Hitre, J. Zaluski, C.R. Chang Chien, A. Makhson, et al., Cetuximab and chemotherapy as initial treatment for metastatic colorectal cancer, N. Engl. J. Med. 360 (14) (2009) 1408–1417.
[4] D. Cunningham, Y. Humblet, S. Siena, D. Khayat, H. Bleiberg, A. Santoro, et al., Cetuximab monotherapy and cetuximab plus irinotecan in irinotecan-refractory metastatic colorectal cancer, N. Engl. J. Med. 351 (4) (2004) 337–345.
[5] W. De Roock, V. De Vriendt, N. Normanno, F. Ciardiello, S. Tejpar, KRAS, BRAF, PIK3CA, and PTEN mutations: implications for targeted therapies in metastatic colorectal cancer, Lancet Oncol. 12 (6) (2011) 594–603.
[6] A. Bertotti, E. Papp, S. Jones, V. Adleff, V. Anagnostou, B. Lupo, et al., The genomic landscape of response to EGFR blockade in colorectal cancer, Nature 526 (7572) (2015) 263–267.
[7] E. Medico, M. Russo, G. Picco, C. Cancelliere, E. Valtorta, G. Corti, et al., The molecular landscape of colorectal cancer cell lines unveils clinically actionable kinase targets, Nat. Commun. 6 (2015) 7002.
[8] K. Imkeller, G. Ambrosi, N. Klemm, A. Claveras Cabezudo, L. Henkel, W. Huber, et al., Metabolic balance in colorectal cancer is maintained by optimal Wnt signaling levels, Mol. Syst. Biol. 18 (8) (2022) e10874.
[9] K. Satoh, S. Yachida, M. Sugimoto, M. Oshima, T. Nakagawa, S. Akamoto, et al., Global metabolic reprogramming of colorectal cancer occurs at adenoma stage and is induced by MYC, Proc. Natl. Acad. Sci. U. S. A. 114 (37) (2017) E7697–E7706.
[10] S. La Vecchia, C. Sebastian, Metabolic pathways regulating colorectal cancer initiation and progression, Semin. Cell Dev. Biol. 98 (2020) 63–70.
[11] S.M. Fendt, C. Frezza, A. Erez, Targeting metabolic plasticity and flexibility dynamics for cancer therapy, Cancer Discov. 10 (12) (2020) 1797–1807.
[12] J. Hirpara, J.Q. Eu, J.K.M. Tan, A.L. Wong, M.V. Clement, L.R. Kong, et al., Metabolic reprogramming of oncogene-addicted cancer cells to OXPHOS as a mechanism of drug resistance, Redox Biol. 25 (2019) 101076.
[13] A. Aloia, D. Mullhaupt, C.D. Chabbert, T. Eberhart, S. Fluckiger-Mangual, A. Vukolic, et al., A fatty acid oxidation-dependent metabolic shift regulates the adaptation of BRAF-mutated melanoma to MAPK inhibitors, Clin. Cancer Res. 25 (22) (2019) 6852–6867.
[14] A. Talebi, J. Dehairs, F. Rambow, A. Rogiers, D. Nittner, R. Derua, et al., Sustained SREBP-1-dependent lipogenesis as a key mediator of resistance to BRAF-targeted therapy, Nat. Commun. 9 (1) (2018) 2500.
[15] W.W. Feng, O. Wilkins, S. Bang, M. Ung, J. Li, J. An, et al., CD36-Mediated metabolic rewiring of breast cancer cells promotes resistance to HER2-targeted therapies, Cell Rep. 29 (11) (2019) 3405–34020 e5.
[16] R.H. Whitehead, F.A. Macrae, D.J. St John, J. Ma, A colon cancer cell line (LIM1215) derived from a patient with inherited nonpolyposis colorectal cancer, J. Natl. Cancer Inst. 74 (4) (1985) 759–765.
[17] S. Misale, R. Yaeger, S. Hobor, E. Scala, M. Janakiraman, D. Liska, et al., Emergence of KRAS mutations and acquired resistance to anti-EGFR therapy in colorectal cancer, Nature 486 (7404) (2012) 532–536.
[18] S. Orjuela, R. Huang, K.M. Hembach, M.D. Robinson, C. Soneson, ARMOR: an automated reproducible MOdular workflow for preprocessing and differential analysis of RNA-seq data, G3 (Bethesda). 9 (7) (2019) 2089–2096.
[19] R. Patro, G. Duggal, M.I. Love, R.A. Irizarry, C. Kingsford, Salmon provides fast and bias-aware quantification of transcript expression, Nat. Methods 14 (4) (2017) 417–419.
[20] C. Soneson, M.I. Love, M.D. Robinson, Differential analyses for RNA-seq: transcript-level estimates improve gene-level inferences, F1000Res 4 (2015) 1521.
[21] M.D. Robinson, D.J. McCarthy, G.K. Smyth, edgeR: a Bioconductor package for differential expression analysis of digital gene expression data, Bioinformatics 26 (1) (2010) 139–140.
[22] H. Tsugawa, T. Cajka, T. Kind, Y. Ma, B. Higgins, K. Ikeda, et al., MS-DIAL: data-independent MS/MS deconvolution for comprehensive metabolome analysis, Nat. Methods 12 (6) (2015) 523–526.
[23] H. Lu, X. Li, Z. Luo, J. Liu, Z. Fan, Cetuximab reverses the Warburg effect by inhibiting HIF-1-regulated LDH-A, Mol. Cancer Therapeut. 12 (10) (2013) 2187–2199.
[24] X. Li, Y. Lu, K. Liang, T. Pan, J. Mendelsohn, Z. Fan, Requirement of hypoxia-inducible factor-1alpha down-regulation in mediating the antitumor activity of the

anti-epidermal growth factor receptor monoclonal antibody cetuximab, Mol. Cancer Therapeut. 7 (5) (2008) 1207–1217.
[25] R.B. Luwor, Y. Lu, X. Li, J. Mendelsohn, Z. Fan, The antiepidermal growth factor receptor monoclonal antibody cetuximab/C225 reduces hypoxia-inducible factor-1 alpha, leading to transcriptional inhibition of vascular endothelial growth factor expression, Oncogene 24 (27) (2005) 4433–4441.
[26] V.L. Payen, E. Mina, V.F. Van Hee, P.E. Porporato, P. Sonveaux, Monocarboxylate transporters in cancer, Mol. Metabol. 33 (2020) 48–66.
[27] M.J. Ovens, A.J. Davies, M.C. Wilson, C.M. Murray, A.P. Halestrap, AR-C155858 is a potent inhibitor of monocarboxylate transporters MCT1 and MCT2 that binds to an intracellular site involving transmembrane helices 7-10, Biochem. J. 425 (3) (2010) 523–530.
[28] C. Vander Linden, C. Corbet, E. Bastien, R. Martherus, C. Guilbaud, L. Petit, et al., Therapy-induced DNA methylation inactivates MCT1 and renders tumor cells vulnerable to MCT4 inhibition, Cell Rep. 35 (9) (2021) 109202.
[29] K. Birsoy, T. Wang, R. Possemato, O.H. Yilmaz, C.E. Koch, W.W. Chen, et al., MCT1-mediated transport of a toxic molecule is an effective strategy for targeting glycolytic tumors, Nat. Genet. 45 (1) (2013) 104–108.
[30] X. Li, Y. Yang, B. Zhang, X. Lin, X. Fu, Y. An, et al., Lactate metabolism in human health and disease, Signal Transduct. Targeted Ther. 7 (1) (2022) 305.
[31] J.C. Marine, S.J. Dawson, M.A. Dawson, Non-genetic mechanisms of therapeutic resistance in cancer, Nat. Rev. Cancer 20 (12) (2020) 743–756.
[32] J. Zhou, Q. Ji, Q. Li, Resistance to anti-EGFR therapies in metastatic colorectal cancer: underlying mechanisms and reversal strategies, J. Exp. Clin. Cancer Res. 40 (1) (2021) 328.
[33] C.M. Parseghian, R. Sun, M. Woods, S. Napolitano, H.M. Lee, J. Alshenaifi, et al., Resistance mechanisms to anti-epidermal growth factor receptor therapy in RAS/RAF wild-type colorectal cancer vary by regimen and line of therapy, J. Clin. Oncol. 41 (3) (2023) 460–471.
[34] L.A. Diaz Jr., R.T. Williams, J. Wu, I. Kinde, J.R. Hecht, J. Berlin, et al., The molecular evolution of acquired resistance to targeted EGFR blockade in colorectal cancers, Nature 486 (7404) (2012) 537–540.
[35] Y. Lu, X. Zhao, Q. Liu, C. Li, R. Graves-Deal, Z. Cao, et al., lncRNA MIR100HG-derived miR-100 and miR-125b mediate cetuximab resistance via Wnt/beta-catenin signaling, Nat. Med. 23 (11) (2017) 1331–1341.
[36] Y. Xiao, T.J. Yu, Y. Xu, R. Ding, Y.P. Wang, Y.Z. Jiang, et al., Emerging therapies in cancer metabolism, Cell Metabol. 35 (8) (2023) 1283–1303.
[37] Z.E. Stine, Z.T. Schug, J.M. Salvino, C.V. Dang, Targeting cancer metabolism in the era of precision oncology, Nat. Rev. Drug Discov. 21 (2) (2022) 141–162.
[38] M. Apicella, E. Giannoni, S. Fiore, K.J. Ferrari, D. Fernandez-Perez, C. Isella, et al., Increased lactate secretion by cancer cells sustains non-cell-autonomous adaptive resistance to MET and EGFR targeted therapies, Cell Metabol. 28 (6) (2018) 848–865 e6.
[39] S. Park, C.Y. Chang, R. Safi, X. Liu, R. Baldi, J.S. Jasper, et al., ERRalpha-regulated lactate metabolism contributes to resistance to targeted therapies in breast cancer, Cell Rep. 15 (2) (2016) 323–335.
[40] E.M.E. Barnes, Y. Xu, A. Benito, L. Herendi, A.P. Siskos, E.O. Aboagye, et al., Lactic acidosis induces resistance to the pan-Akt inhibitor uprosertib in colon cancer cells, Br. J. Cancer 122 (9) (2020) 1298–1308.
[41] L. Pisarsky, R. Bill, E. Fagiani, S. Dimeloe, R.W. Goosen, J. Hagmann, et al., Targeting metabolic symbiosis to overcome resistance to anti-angiogenic therapy, Cell Rep. 15 (6) (2016) 1161–1174.
[42] A.J. Monteith, H.E. Ramsey, A.J. Silver, D. Brown, D. Greenwood, B.N. Smith, et al., Lactate utilization enables metabolic escape to confer resistance to BET inhibition in acute myeloid leukemia, Cancer Res. 84 (7) (2024) 1101–1114.
[43] H. Wu, Z. Ding, D. Hu, F. Sun, C. Dai, J. Xie, et al., Central role of lactic acidosis in cancer cell resistance to glucose deprivation-induced cell death, J. Pathol. 227 (2) (2012) 189–199.
[44] M.L. McCleland, A.S. Adler, L. Deming, E. Cosino, L. Lee, E.M. Blackwood, et al., Lactate dehydrogenase B is required for the growth of KRAS-dependent lung adenocarcinomas, Clin. Cancer Res. 19 (4) (2013) 773–784.
[45] J.R. Doherty, C. Yang, K.E. Scott, M.D. Cameron, M. Fallahi, W. Li, et al., Blocking lactate export by inhibiting the Myc target MCT1 Disables glycolysis and glutathione synthesis, Cancer Res. 74 (3) (2014) 908–920.
[46] H. Sabe, KRAS, MYC, and ARF6: inseparable relationships cooperatively promote cancer malignancy and immune evasion, Cell Commun. Signal. 21 (1) (2023) 106.
[47] E. Kerkhoff, R. Houben, S. Loffler, J. Troppmair, J.E. Lee, U.R. Rapp, Regulation of c-myc expression by Ras/Raf signalling, Oncogene 16 (2) (1998) 211–216.
[48] Z. Tong, X. Wang, S. Shi, T. Hou, G. Gao, D. Li, et al., Development of lactate-related gene signature and prediction of overall survival and chemosensitivity in patients with colorectal cancer, Cancer Med. 12 (8) (2023) 10105–10122.
[49] W.H. Yang, Y. Qiu, O. Stamatatos, T. Janowitz, M.J. Lukey, Enhancing the efficacy of glutamine metabolism inhibitors in cancer therapy, Trends Cancer 7 (8) (2021) 790–804.
[50] A.S. Cohen, L. Geng, P. Zhao, A. Fu, M.L. Schulte, R. Graves-Deal, et al., Combined blockade of EGFR and glutamine metabolism in preclinical models of colorectal cancer, Transl Oncol 13 (10) (2020) 100828.
[51] H. Ma, Z. Wu, J. Peng, Y. Li, H. Huang, Y. Liao, et al., Inhibition of SLC1A5 sensitizes colorectal cancer to cetuximab, Int. J. Cancer 142 (12) (2018) 2578–2588.
[52] C. Vander Linden, C. Corbet, Reconciling environment-mediated metabolic heterogeneity with the oncogene-driven cancer paradigm in precision oncology, Semin. Cell Dev. Biol. 98 (2020) 202–210.